CHAPTER IV

THE RADIO CORES OF GIANT RADIO GALAXIES

4.1 INTRODUCTION:

As outlined in the introductory chapter we are attempting to investigate the various possible factors responsible for the exceptionally large physical sizes of the giant radio galaxies. Here we examine the possible link of the nuclear activity to the GRG phenomenon.

The properties of the central object in double radio sources have been studied by many authors. Yee and Oke (1978) made spectrophotometric observations of some 3CR galaxies, which showed that the nuclear emission line strengths and nuclear non-thermal optical emission correlate with the nuclear radio emission. Correlations between the total optical luminosity of the parent galaxy, the total radio luminosity of the extended radio structure and the nuclear X-ray luminosity with the core radio luminosity have also been found (Fabbiano et al., 1984; Feigelson and Berg, 1983; Yee and Oke, 1978; Hine and Longair, 1979; Burns et al., 1984). These studies suggest that the core radio luminosity in double radio sources may be an indicator of the beam power from the central engine (Burns et al., 1984). It is therefore relevant to study the core properties in GRGs to determine the extent to which they may be responsible for their large physical sizes.

Radio cores have been detected so far in 13 of the 15 GRGs in our sample. Since the GRGs constitute the extreme end of the linear size distribution for radio galaxies, a large fraction of them is expected to have the main axis close to the plane of the sky. Projection effects are therefore likely to be quite small compared to any other known sample of radio sources. The observed parameters should thus be close to the intrinsic (i.e., projection free) parameters, in a statistical sense (Saripalli et al., 1986; Saripalli and Gopal-Krishna, 1987).

In this chapter we have made a statistical comparative study of (a) the radio powers of the cores and (b) the 'core-fraction' defined as the ratio of the core flux at 5 GHz and the total flux at 408 MHz, for our sample of 12 GRGs with detected cores (excluding the giant quasar), vis-a-vis a carefully selected sample of 35 normal size sources. Effects of projection which could be prevalent in this comparision sample have been considered while interpreting the results. Since the radio luminosity of the core is found to correlate with the optical luminosity of the parent galaxy (Fabbiano et al., 1984; Ulrich and Meier, 1984; Feretti et al., 1984) we have compared the absolute visual magnitudes of the parent galaxies in the two samples to look for any such biases affecting our results.

4.2 SAMPLE SELECTION

In the GRG sample, we include all GRGs (the quasar, 4C34.47, has been excluded as quasars are believed to have core properties different from radio galaxies) except the two southern sources 0114-476 and 0211-479 for which the available observations do not reveal any cores (most probably due to their poor resolution). This leaves 12 GRGs with detected radio cores whose properties are summarized in Table 4.1. Column 1, gives the IAU name and any other name; Column 2, gives the redshift; Column 3, the largest linear size, Column 4, the Fanaroff-Riley (FR) classification for the structure; Column 5, the total flux at 408 MHz, Column 6, the total power at 408 MHz; Column 7, gives the core flux at 5 GHz; Column 8, the core power at 5 GHz; Column 9, the derived absolute visual magnitude of the parent galaxy. The apparent magnitudes used for computing M_V have been taken from the available literature (see Chapter II, Table 2.5); Column 10, the fractional flux in the core in percentage, defined as $f_c = S^c_{5000}/S^t_{408}$, and Column 11, gives the reference codes for data on cores. The core fraction f_c is essentially free of effects of K-correction due to the small redshifts ($z<0.25$) of the galaxies in the two samples. The K-correction would tend to increase the value of f_c because of the difference in the spectral slopes of the core and the extended structure.

While for most GRGs the values of core fluxes at 5 GHz have been taken from the literature (Saripalli et al., 1986 and references therein), for three GRGs these have come from our own observations. We observed the central regions of 4C39.04, 0503-286 (Chapter II) and 4C73.08 at 5 GHz with the

VLA as part of our effort to improve the radio data on GRGs. The radio maps of the central regions of these GRGs are shown in Fig.2.2 (Chapter II), and Fig.4.1, and the observational details are given in Table 4.3.

The GRG sample has the following characteristics: $z < 0.22$; $10^{25} < P_{408} < 10^{27}$ WHz^{-1}; and having a galaxy identification. We have, therefore, chosen a comparison sample matching these selection criteria but restricted to the range 100 to 500 kpc in largest linear size (LLS) from the 'composite' sample of Feretti et al. (1984). The latter was derived from the B2 bright, B2 faint and 3CR samples of radio galaxies. The comparison sample, thus selected, contains 35 sources (Table 4.2).

Radio structures for most sources in the comparison sample were taken from the recently published VLA observations of B2 sources (Parma et al. 1986; de Ruiter et al., 1987; Fanti et al., 1986 and Fanti et al., 1987, hereafter papers I, II, III and IV respectively). For the remaining (mostly 3CR) sources relevant data were taken from the available highest resolution observations from literature. References for structure are given in the last column of Table 4.2 formatted similar to Table 4.1. The maximum of the linear size range adopted for defining the comparison sample (500 kpc) permits the comparative study with GRGs to be made over a sufficiently large size ratio. The lower limit of 100 kpc was chosen on the consideration that the sources are not

Table 4.1: The GRG Sample

Name	z	LLS Mpc	FR Class	S^t_{408} Jy	P^t_{408} 10^{26} WHz^{-1}	S^c_{5000} Jy	P^c_{5000} 10^{24} WHz^{-1}	M_v	f_c %	Ref.codes
0055 + 300 NGC315	0.0167	1.7	II	9.6	0.1	0.62	0.74	-23.6	6.46	BF79
0114 - 476	0.146	2.0	II	10.4	10	-	-	-22.6	-	
0136 + 396 4C39.04	0.2107	2.0	II	3.3	8.0	0.011	2.6	-22.2	0.33	*
0157 + 405 4C40.08	0.078	1.7	I/II	4.9	1.5	~0.005	0.14	-22.8	0.10	F86
0211 - 479	0.22	1.6	II	3.4	8.5	-	-	-23.7	-	
0448 + 519 3C130	0.1090	1.9	I	8.9	5.0	0.028	1.5	-22.7	0.31	vB86
0503 - 286	0.038	2.5	II	10.5	0.7	0.006	0.038	-21.1	0.06	*
0744 + 559 DA240	0.0356	2.0	II	16.3	0.9	0.111	0.62	-21.6	0.68	S86
0945 + 734 4C73.08	0.0581	1.7	II	7.7	1.2	0.011	0.16	-23.1	0.14	*
1003 + 351 3C 236	0.0988	5.8	II	10.9	4.9	1.5	67.3	-23.2	13.76	S86
1331 - 099	0.081	1.6	II	6.7	2.0	0.09	2.6	-20.3	1.34	S86
1452 - 518	(0.08)	2.5	I/II	4.7	1.4	0.135	3.7	-22.9	2.9	J86
1549 + 202 3C326	0.0895	2.7	II	10.6	4.0	0.013	0.46	-22.3	0.12	S86
1637 + 826 NGC6251	0.023	2.0	II	5.5	0.1	0.9	2.05	-22.9	16.3	S86

Footnotes: BF79: Bridle and Fomalont,1979; *:present work; F86:Faulkner,Ph.D Thesis 1986; vB:van Breugel et al.,1986; S86:Saripalli et al.,1986; J86: Jones,1986.

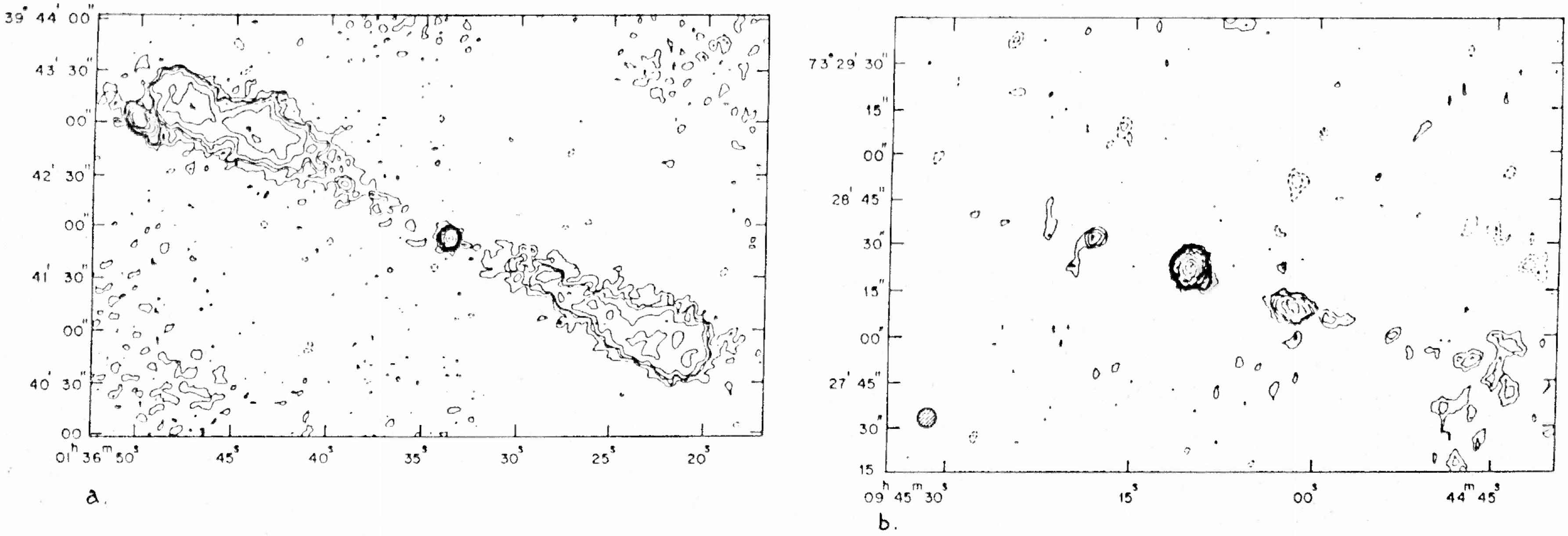

Table 4.3 Core observations

Name	Beam (" arc)	core S_5 (mJy)	Rms Noise (mJy)
4C39.04	6 x 6	10.9	0.10
0503-286	4 x 4	6.4	0.05
4C73.08	6 x 6	10.7	0.13

Fig.4.1(a) Total intensity distribution of 4C39.04 at 5 GHz observed with the VLA. The restoring beam has a FWHM 6" x 6" arc. The contours are at -0.15, 0.15, 0.3, 0.4, 0.6, 1.0, 1.5, 2.0, 4.0, 7.0, 10.0 mJy/beam. (b) The total intensity distribution of the radio core of 4C73.08 at 5 GHz observed with the VLA. The restoring beam has a FWHM 6"x6" arc. Contours are at -0.4, -0.3, 0.3, 0.4, 0.5, 0.6, 0.8, 1.0, 1.2, 1.5, 2.0, 3.0, 4.0, 6.0, 8.0, 10.0 mJy/beam.

Table 4.2: The Comparision Sample

Name	z	LLS Kpc	FRI/II	S^{t}_{408} Jy	P^{t}_{408} $10^{26}WHz^{-1}$	S^{c}_{5000} Jy	P^{c}_{5000} $10^{24}WHz^{-1}$	M_v	f_c %	Ref.Codes
0053 + 261 3C28	0.1952	220	II	7.3	12	< 0.01	< 1.75	-23.47	< 0.14	F84
0055 + 26 NGC326	0.0472	212	II/Inv. Sym.	4.9	0.5	< 0.01	< 9.7	-23.6	< 0.2	E81
0106 + 130 3C33	0.0595	394	II	31.6	4.8	0.024	0.37	-22.77	0.08	F84
0220 + 427 3C66B	0.0215	148	I	19.23	0.38	0.160	0.32	-22.96	0.8	F84
0300 + 162 3C76.1	0.0328	130	I	5.1	0.24	0.001	0.047	-21.77	0.2	F84
0356 + 102 3C98	0.0306	254	II	25.3	1.0	0.009	0.037	-22.04	0.04	F84
0734 + 805 3C184.1	0.1182	486	II	7.6	4.6	0.006	0.37	-22.67	0.08	F84
0802 + 243 3C192	0.0597	300	II/Inv. Sym.	12.2	1.9	0.008	0.13	-22.6	0.07	F84
0828 + 32 AB	0.0507	438	II	4.37	0.48	< 0.003	< 0.034	-22.5	< 0.07	II
0836 + 29	0.0790	366	II	1.8	0.48	0.075	2.1	-23.97	4.2	II,III
0908 + 37	0.1040	133	II	1.19	0.55	0.017	0.82	-23.79	1.4	I,III
0922 + 36B	0.1125	466	II?	1.82	1.0	0.006	0.34	-23.89	0.33	II,III
1102 + 30	0.0720	321	II	0.96	0.20	0.0068	0.16	-23.8	0.71	II,III
1113 + 29	0.0489	121	II	4.95	0.50	0.023	0.24	-23.41	0.46	I,III
1204 + 34	0.0788	104	II	1.01	0.27	0.008	0.22	-22.79	0.79	I,III
1251 + 27 3C277.3	0.0857	99	II	6.3	2.0	0.020	0.65	-22.58	0.32	F84
1319 + 428 3C285	0.0797	275	II	5.6	1.5	0.006	0.17	-22.62	0.11	F84
1347 + 28	0.0724	170	II	0.52	0.12	0.0023	0.053	-23.18	0.44	I,III
1350 + 31 3C293	0.0452	131	I/Inv. Sym.	10.15	0.9	1.36	12	-22.97	13.4	B81
1357 + 28	0.0629	232	II ?	0.690	0.12	0.0046	0.08	-23.45	0.67	II,III
1414 + 110 3C296	0.0237	243	I	6.8	0.16	0.077	0.19	-23.62	1.1	F84
1441 + 26	0.0621	157	II	0.66	0.11	< 0.002	< 0.032	-23.7	< 0.3	II
1450 + 28	0.1265	163	I	0.38	0.26	0.0041	0.29	-23.25	1.1	I,III
1502 + 26 3C310	0.0540	300	I	23.4	2.9	0.080	1.02	-22.79	0.34	F84
1521 + 28	0.0825	426	I	1.57	0.46	0.03	1.3	-23.29	1.9	II,III
1615 + 32 3C332	0.1515	322	II	6.8	6.8	0.0075	0.78	-23.54	0.11	II
1643 + 27	0.1017	359	II	0.290	0.13	0.003	0.14	-23.46	1.03	II,III
1658 + 30	0.0351	155	II	1.55	0.082	0.04	0.21	-21.69	2.6	II,III

1726 + 31 3C357	0.1670	414	II	6.15	7.3	0.005	0.63	-24.17	0.08	II,III
1832 + 474 3C381	0.1605	270	II	10.0	11	0.005	0.58	-23.29	0.05	F84
1833 + 32 3C382	0.0586	282	II	13.7	2.0	0.190	2.9	-23.7	1.4	I
1842 + 455 3C388	0.0917	105	II	14.6	5.0	0.062	2.3	-23.81	0.42	F84
1845 + 797 3C390.3	0.0569	331	II	26.9	3.7	0.33	4.7	-23.45	1.2	F84
2212 + 137 3C442	0.0262	197	I	10.6	0.31	0.002	0.006	-22.48	0.02	F84
2229 + 39 3C449	0.0181	456	I	6.45	0.09	0.037	0.053	-21.9	0.57	E81

Footnotes: F84: Feretti et al., 1984; E81: Ekers et al., 1981; I: Parma et al., 1986; II:de Ruiter et al., 1987; III: Fanti et al., 1986; IV: Fanti et al., 1987; B81: Bridle et al., 1981

Table 4.4:The Optical Spectral data of GRGS

Name	z	FRI/II	P^t_{408} 10^{26} WHz^{-1}	P^n_{5000} 10^{24} WHz^{-1}	Em.Lines	Reference
0055 + 300 NGC315	0.0167	II	0.1	0.74	X	G81,BC86
0114 - 476	0.146	II	10		✓	DG83
0136 + 396 4C39.04	0.2107	II	8.0	2.6	✓	H79
0157 + 405 4C40.08	0.078	I/II	1.5	0.14	-	-
0211 - 479	0.22	II	8.5		✓(SE)	D78
0448 + 519 3C130	0.1090	I	5.0	1.5	X	G81,BC86
0503 - 286	0.038	II	0.7	0.038	✓(SE)	S86
0744 + 559 DA240	0.0356	II	0.9	0.62	✓	S82
0945 + 734 4C73.08	0.0581	II	1.2	0.16	✓(SE)	D70
1003 + 351 3C236	0.0988	II	4.9	67.3	✓	MO79
1331 - 099	0.081	II	2.0	2.6	X	D78
1452 - 518	(0.08)	I/II	1.4	3.7	-	-
1549 + 202 3C326	0.0895	II	4.0	0.46	X	WS78
1637 + 826 NGC6251	0.023	II	0.1	2.05	✓	MO79

G81: Guthrie,1981; BC86: Burbidge and Crowne,1986; DG83: Danziger and Goss, 1983; H79: Hine,1979; D78: Danziger et al.,1978; S86: Saripalli et al.,1986; S82: Saunders, 1982; D70: Demouline-Ulrich,1970; MO79: Miley and Osterbrock,1979; WS78: Willis and Strom,1978.

subgalactic and, moreover, are adequately resolved, for reliable measurement of the cores.

The core fraction has been defined as $S^{core}_{5000}/S^{total}_{408}$ rather than $S^{core}_{5000}/S^{total}_{5000}$ for the reasons spelled out by Feretti et al.: The lobes are more easily seen at low frequencies whereas the existing maps at 5 GHz miss out substantial amount of lobe flux. In contrast, the cores are more easily detected at the higher frequency due to their flat spectrum, aided by the angular resolution.

The absolute visual magnitude for the galaxies in both the samples have been calculated from the available apparent magnitudes, after applying K-correction and correction for the galactic absorption (Feretti et al., 1984; Chapter II, Table 2.5). Values for the K corrections were adopted from Whitford (1971), while the correction for the galactic absorption were made using the following relations taken from Sandage (1973): A_B = 0.132 (cosec b-1); A_V = 0.10 (cosec b-1) and A_R = 0.071 (cosec b-1) for $|b| \leq 50^o$, and $A_B = A_V = A_R$ = 0 for $|b| \geq 50^o$. We also used the following relations: m_B = m_{pg} + 0.11, (Lang, 1978); B-V = 0.976 and V-R = 0.861 (Sandage, 1973).

The apparent magnitudes of the sources in the comparison sample taken from the B2 faint subsample are expected to be in error by ±0.2 magnitude (Fanti et al., 1978). The magnitudes for those taken from the B2 bright subsample have been taken from the Catalogue of Galaxies and Clusters of

Galaxies (Zwicky and Herzog, 1963) and are also expected to be uncertain by ± 0.2 mag. For most of the (15) 3CR galaxies in the comparison sample photoelectric magnitudes are available (Laing, Riley and Longair, 1983), except for 3C184.1. The magnitude for this source is given by Smith and Spinrad (1980), with a quoted error of 0.5-1 magnitude. Overall, the magnitudes of the sources in the comparison sample have been fairly well estimated. Unfortunately, for GRGs, such precise data are not available; the quoted magnitude errors are 0.5 to 1.

For 16 out of 35 sources in the comparison sample, the core fluxes have been translated to 5 GHz, assuming $\alpha = ^{core} +0.3$ ($S_\nu \propto \nu^{-\alpha}$) from the tabulated values at 1.4 GHz, based on arcsecond to a few arcsecond-resolution VLA data (Paper IV). For the remaining, which are mostly 3CR sources, the core fluxes have been taken from somewhat lower (few-arcsecond) resolution maps made with the Cambridge 5-Km telescope, VLA or WSRT at 5 GHz and are, hence, likely to be over-estimated. Feretti et al. (1984) have estimated the over-estimate to be $\sim$ 40%. This is most significant for FRI type sources, where the twin jets are seen adjacent to the core. In comparison, the GRGs have been observed with a significantly larger number of beam elements over their lengths (on the average, by a factor of 10 or more), so the core fluxes are much less likely to have been significantly be over-estimated (see below).

4.3 RESULTS AND DISCUSSION

The results of the comparison of the core powers, core fractions and absolute (visual) magnitudes for the GRGs and the comparison sample are presented in the form of histograms in Fig.4.2. From Fig.4.2(a) it is seen that the distributions of the core fractions in the GRG and the comparison samples are quite similar. The median value of f_c for GRGs is 0.83% and that for the comparision sample is in the range 0.50 $\pm$ 0.05%. The error only refers to varying f_c between 0 and the upper limit in all cases where only upper limits to f_c are known. To determine the effect of inclusion of the FRI sources, we have shown them as hatched regions. It is found that excluding FRI sources does not substantially alter the f_c distributions, the median core-fractions for the two samples now becomming 0.9% and 0.38 $\pm$ 0.08%, respectively.

The distribution of the 5 GHz core powers for the two samples are shown in Fig.4.2(b). The cores of the GRGs are definitely as powerful or more powerful than those in the normal size sources. The median core power (at 5 GHz) for the GRGs is 10^{24} WHz^{-1} for GRGs and 3.10^{23} WHz^{-1} for the comparison sample.

Fig.4.2(c) shows the distributions of the absolute visual magnitudes of the parent galaxies in the two samples. It is seen that the parent galaxies of GRGs are at most as luminous (median M_V = -22.7) as those of the normal size sources (median M_V = -23.2) in the comparison sample, even

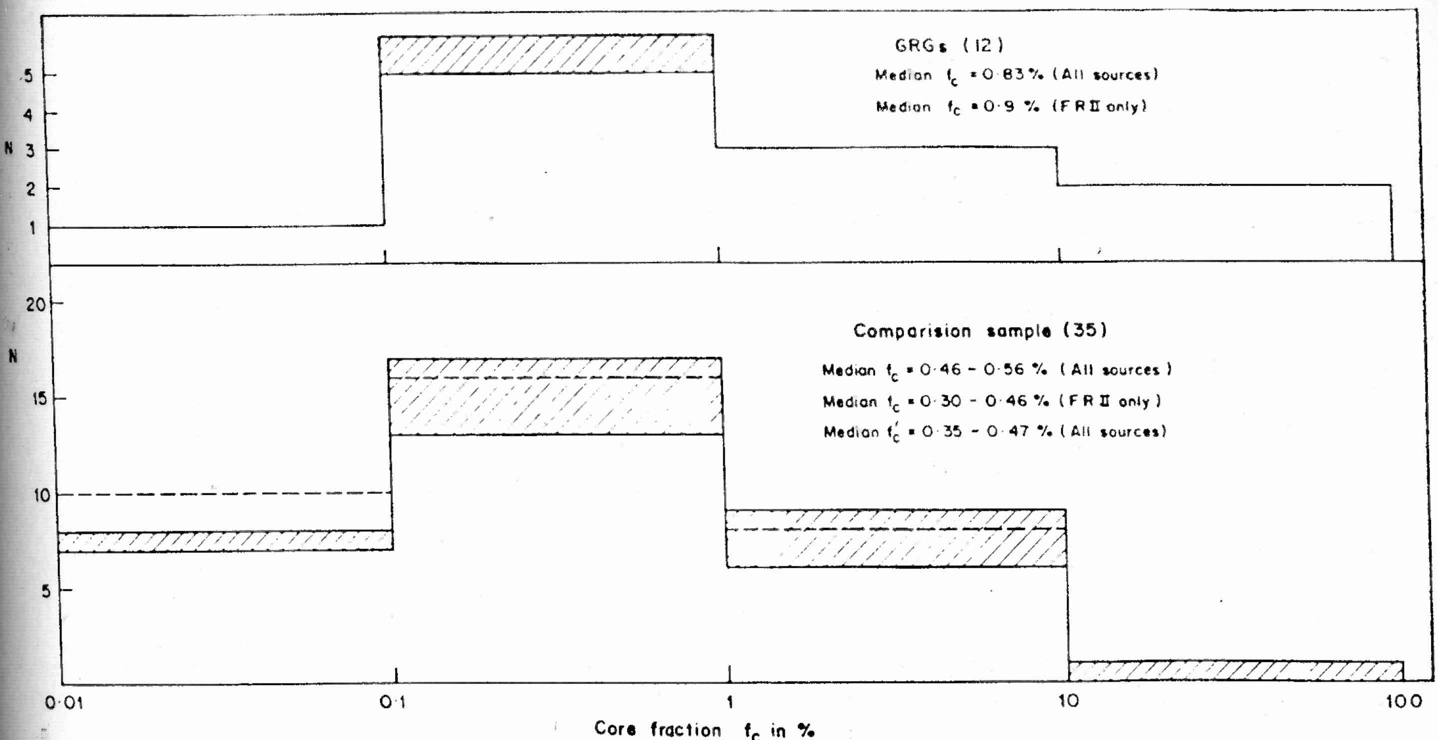

Fig.4.2(a) Distribution of the core-fraction, f_c (= core flux at 5000 MHz/total flux at 408 MHz), for the sources in the GRG and the comparison samples. Values corresponding to FRI type sources are shown hatched. f'_c is the median core-fraction for the comparison sample when the core fluxes of 16 sources observed with few arc-second resoltuions are reduced by 36% (see Section 4.2); dashed lines indicate the resulting distribution.

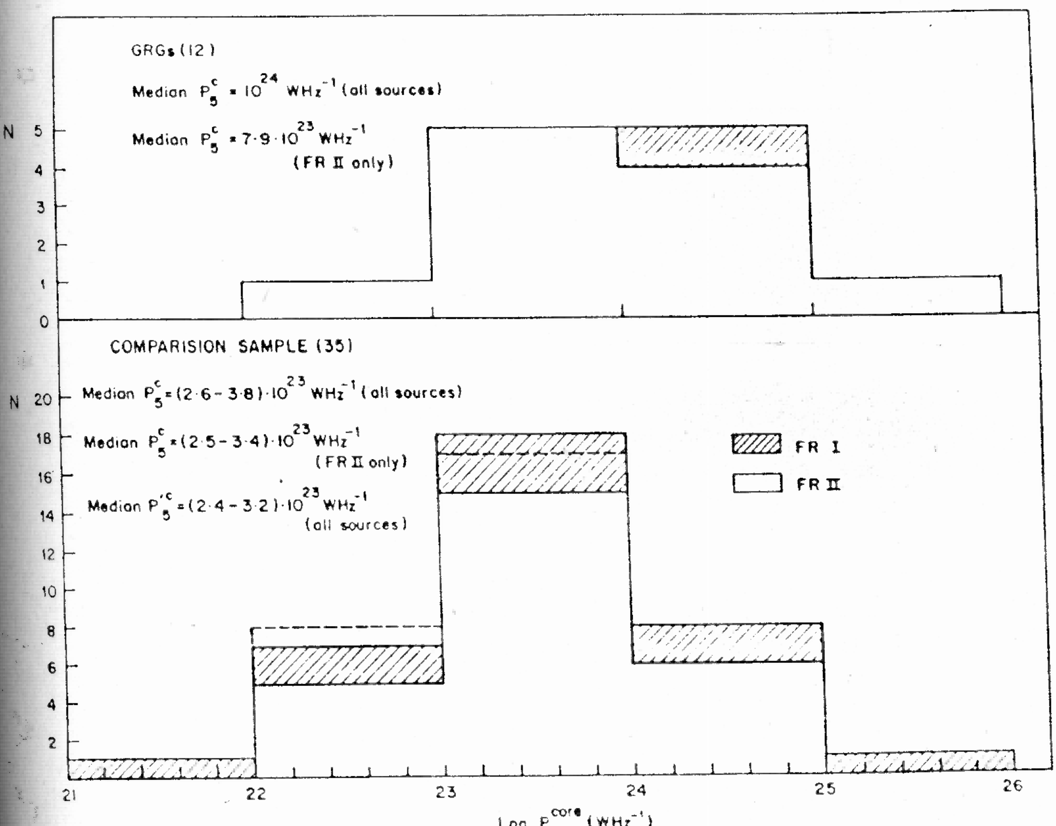

Fig.4.2(b) Distribution of the core power, P_5^{core} at 5 GHz, for the sources in the GRG and the comparison samples. Hatched regions indicate value for FRI type sources.

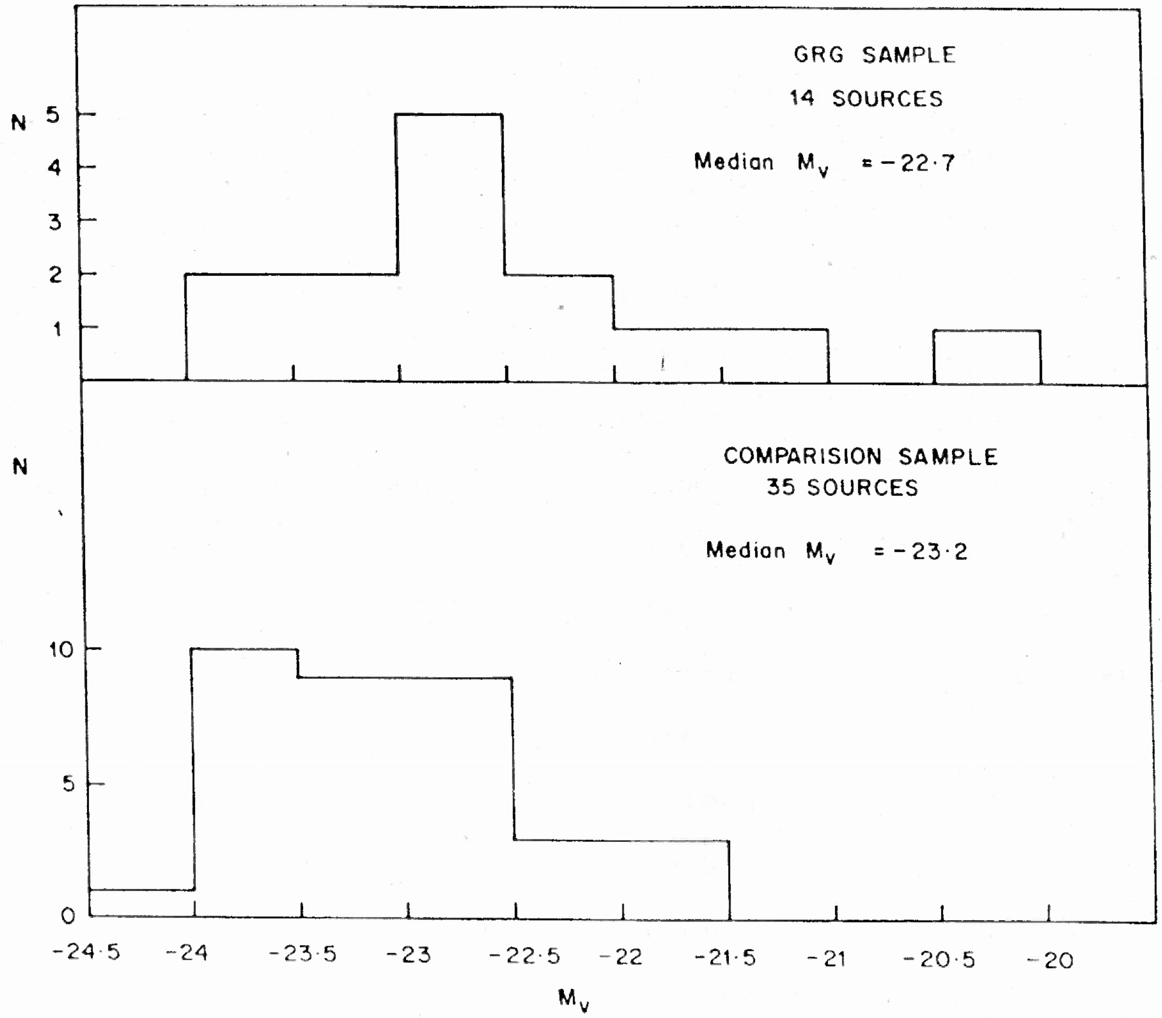

Fig.4.2(c) Distribution of the absolute visual magnitude, M_V of the parent galaxies of the sources in the GRG and comparison samples.

considering the relatively large uncertainty associated with the values of M_V available for GRGs.

The distributions of core fraction and core powers for the two samples compared above, have yielded rather unexpected results. The radio cores of GRGs are found to be as powerful and as prominent, if not more, as the cores of normal size double sources belonging to the same range of total radio power and redshift. Neglect of the FRI type sources in the two distributions does not affect the results appreciably. We shall discuss the significance of the results keeping in mind the following biases:

a. The data for the GRGs has been taken from maps which have, on the average, at least 10 times more number of beams across the source's length than even the 16 sources in the comparison sample observed with the highest (arcsecond) resolution. For the remaining 19 sources in the comparison sample, the situation is worse, since the core fluxes adopted from Feretti et al. (1984) have been derived from several-arcsecond-resolution maps. Arcsecond resolution data available for the 11 FRII sources in the comparison sample when compared with their older few-acrsecond resolution data, shows a 36% over estimate in the older estimates of core flux.

b. The sources in the comparison sample have been selected from samples observed at low frequencies and are therefore expected to be randomly oriented with respect to the line of sight. Allowing for this, will further reduce the intrinsic core powers and core-fractions of some of the sources, whose core flux may have been boosted due to relativistic beaming. Much less of such boosting is expected for the GRGs (Section 4.1)

The similarity in the distributions of the core powers and core-fractions of the GRGs and the comparison sample, despite the above mentioned biases could still be understood if the parent galaxies of GRGs were optically more luminous than those of the comparison sources (see Fabbiano et al., 1984; Ulrich and Meier, 1984 and Feretti et al., 1984). Comparison of the absolute magnitudes of the two samples (Fig.4.2c) shows no evidence for the parent galaxies of GRGs being more luminous even allowing for relatively larger errors in their published magnitudes.

From considerations of the evolution of the double sources, GRGs are probably older objects, statistically, than the normal size sources (Chapter II). Hence, one would expect the activity in the cores of GRGs to have diminished over the long lifetime. This is not indicated by the results presented here.

We have shown from our statistical study that compared to a redshift and radio luminosity matched sample of normal size sources,GRGs possess intrinsically more powerful and prominent radio cores. This is indicative of more powerful and longer lived central engines in the GRGs, which are then likely to be a key factor behind the formation of such enormously large radio sources. This, result is further strengthened by the conclusion arrived at in Chapter VI, from dynamical arguments.

From the work of Yee and Oke (1978), Hine and Longair (1979) and Fabbiano et al. (1984) it is known that stronger radio cores are accompanied by stronger optical emission lines, higher optical non-thermal content, and larger X-ray power from the nucleus. From our finding that GRGs possess strong radio cores, indicating large power of the central engine, it is expected that they also conform to the properties stated above. Such a study is only possible at present in terms of a broad classification of the optical spectral 'type', since the details of optical spectra are generally not available in literature. We have tabulated in Table 4.3, the spectral classification, together with brief comments on the optical spectra for the 12 GRGs, compiled from the published literature.

Here it must be mentioned that Saunders (1982) suggested a re-classification of the optical spectra of 6 GRGs, and concluded a high occurrence rate of class A (or strong emission line spectra) among them, contrary to earlier indications (Hine and Longair, 1979). Although the re-classification scheme of Saunders' is an attempt at quantifying the spectral classification scheme of Hine and Longair, it is a poor substitute for the actual line strengths, as pointed out by him. Moreover, any comparison of strengths becomes meaningful only if all the source spectra are obtained with similar spatial and frequency resolution as well as atmospheric conditions.

Confining ourselves to merely the reported presence or absence of emission lines, our compilation of the optical spectral characteristics of the 12 GRGs (Table 4.4) reveals 8 GRGs showing emission lines and 4 lacking them. Among the 8 GRGs with detected emission lines, only 3 have been explicitly classified by the respective observers as strong emission line galaxies (type A, Table 4.4). Although a re-examination of the spectra on the lines of Saunders (1982), and more sensitive high resolution optical observations (which is planned) could reveal additional class 'A' cases among these GRGs, it is significant that (a) no emission lines have been detected in 4 out of 12 GRGs and (b) atleast 4 have been classified as yet as class B type (having weak or no emission lines, Table 4.4).

If, as concluded in this chapter as well as, in Chapter III and Chapter VI, the exceptional sizes of GRGs are due to powerful central engines, and if the core radio power is an indicator of the strength of the central engine (see Section 4.1), a high incidence of strong optical line emission (Class A) would be expected. As yet, such a trend is not discerned from the compilation of the available optical data for the 12 GRGs, though the situation may change when improved optical spectra become available (eg., Saunders, 1982).

Any prevalence of weak or no emission line spectra (Class B) among GRGs would indicate that over their long life times of the mechanisms giving rise to the emission lines have either weakened or the gaseous filaments blown off by the sustained nuclear activity. The radio decay could be staggered in time, or the energy spent on the excitation of the emission lines is instead channeled into a "useful" form, like the bulk kinetic energy in the beams, aiding the formation of giant radio sources.

4.4 CONCLUSIONS

By comparing two samples, one consisting of 12 GRGs and the other of 35 normal size radio sources and, at the same time, ensuring that they are well matched in their distributions of redshifts, as well as radio powers, we find that: Statistically, the cores of GRGs appear at least as radio powerful as those of the normal size sources. The latter sources are presumably seen at a younger stage and, moreover, the emission of their cores is more likely to have been boosted due to relativistic beaming, as compared to the cores of GRGs whose axes are expected to be highly misaligned from the line-of-sight. Together, both these effects are expected to have caused the cores of normal size sources to appear brighter. But the present analysis yields no evidence for it. This unexpected behaviour is not likely to be due to an optical bias, since we do not find the parent galaxies of GRGs to be optically more luminous than the parent galaxies of the normal size radio sources. Put together, all these findings seem to support the idea that GRGs are produced by central engines capable of intrinsically stronger and more sustained nuclear acitivity, compared to the normal size double radio sources (see also Chapter VI).

CHAPTER V

THE ENVIRONMENTS OF GIANT RADIO GALAXIES

5.1. INTRODUCTION

Various studies have indicated that nuclear activity in radio galaxies is fostered by a dense (local) galaxy environment (eg., Adams et al., 1980; Sparks et al., 1984; Hutchings et al., 1984; Heckman et al., 1985; Reynolds, 1986). Although the precise mechanism is not clear at present, it is supposed that interactions with the neighbouring galaxies may somehow activate the galactic nucleus by driving an enhanced accretion of extranuclear material on to it. Evidence against such a scenario came from the reported similarity between the radio-optical luminosity functions of cluster and field galaxies (Auriemma et al., 1977; Fanti et al., 1982; Hummel et al., 1983; Brosch and Krumm, 1984). However as noted by Adams et al., (1980), Dressel (1981), and others, cluster membership alone can be a rather poor indicator of the gravitational influence of the surrounding galaxies. The role of the environment does not seem confined to being the trigger for nuclear activity but also appears to influence several observable properties like the morphology, spectrum and overall size of radio galaxies. Even the efficiency of conversion of the beam power into radio emission has been shown to depend on the environment, being higher for a denser ambient medium (eg., Rawlings and Saunders, 1988).

In this chapter we present a study of the environments of giant radio galaxies to determine their role in aiding the formation of exceptional linear sizes. It is known that X-ray observations enable direct detection of the gaseous medium which is likely to have most important influence on the radio lobes. More indirectly, the density of the medium may be inferred, statistically, from the observed degree of clustering of galaxies around the radio source, as pioneered by Stocke (1979); Guindon (1979); Seldner et al., (1977) etc. The former two authors tried to eliminate the cases of chance projection towards a given radio galaxy by only considering the galaxies within appropriate, narrow ranges of optical diameter or apparent magnitude, based on eye estimates. On the other hand, Seldner and Peebles (1978) as well as Longair and Seldner (1979) pioneered the technique of using the 2-point correlation function to quantify the degree of clustering of galaxies around a given object of interest. In particular, Longair and Seldner (1979) devised a scheme for estimating the galaxy density around a given location in space by correcting the observed angular cross-correlation coefficients using the knowledge of galaxy luminosity functions and K-corrections. More recently this approach has been applied to quasars by Yee and Green (1984) and for radio galaxies of different morphologies by Prestage and Peacock 1987 (hereafter PP). The latter authors have shown that core-dominated radio sources and possibly edge-brightened (FRII) radio galaxies are preferentially located in significantly less clustered environments than the edge-darkened (FRI) double radio sources. The different environments for radio galaxies of different morphologies have led to models which require the energy supplying beams to be affected to various degrees by the external gas, depending on the intrinsic power in the beams (eg., Bicknell, 1985; Gopal-Krishna and Wiita, 1988). GRGs have radio power near the transition between FRII and FRI type sources, and therefore it is clearly of interest to examine the degree of clustering characterizing their environments. Intergalactic medium is expected to play a prominent role in shaping the structures of GRGs since their radio lobes are located well outside any gaseous halo associated with the parent galaxy.

In this chapter we shall estimate the spatial covariance function coefficients for 7 of the 14 known GRGs, for which we have obtained the digitisations of their optical plates using the COSMOS measuring machine. Further in an attempt to explore the reason for the markedly unequal lengths of the two radio lobes, observed in most GRGs, we used the above plate material for deducing and comparing the clustering of galaxies at 2 well defined offset positions separated by 1 Mpc from the nucleus of each GRG on opposite sides along the radio axis. These estimates referring to the positions offset from the nucleus are expected to be a more realistic density indicator for the intergalactic medium with which the lobes of the GRGs interact. As discussed in Section 5.2, the concentration of the galaxy distribution, appropriately quantified for 2 offset positions about each of the GRGs, shows an interesting correlation with the observed lengths of the radio lobes. This lends support to the possibility that the galaxy density can be a useful indicator of the density of the gaseous medium interacting with the radio lobes.

5.1.1 Method of Analysis

We have employed the covariance function technique to study the environments of GRGs quantitatively. This method of analysis is discussed in detail by Longair and Seldner (1979) and will only be briefly described here. For any projected distribution of galaxies about a point, the 2-point angular correlation function $\omega(\theta)$ is given by the relation

$$n(\theta)d\Omega = N_g(1 + \omega(\theta))d\Omega \qquad \text{...(5.1)}$$

$n(\theta)d\Omega$ is the number of galaxies in a ring of radius θ and angular area $d\Omega$, centred at the reference point. N_g is the average surface density of galaxies above the plate completeness limit. $\omega(\theta)$ is the additional probability (over the average level) of finding a galaxy at an angular distance of θ from the reference location. It is taken to have a power-law form : $\omega(\theta)=A_{gg}\,\theta^{-\alpha}$, with the exponent α= +0.77 (see Longair and Seldner, 1979; Groth and Peebles, 1977; also see Appendix I of PP).

Use of A_{gg} as a statistic for studying clustering strengths about a chosen reference location is limited. A_{gg} would be indicative of poor clustering strength if a given cluster were at high redshift than if it were at a low redshift. To obtain a factual estimate of the clustering strength a de-projection of the excess counts is carried out, employing the galaxy luminosity functions and K-corrections. This is done by relating the angular covariance function $\omega(\theta)$, to the spatial covariance function $\xi(r) = B_{gg}.r^{-\gamma}$, through the relation (cf., Longair and Seldner, 1979 for a complete description):

$$A_{gg}* = H(z)\ B_{gg}*$$

'*' denoting a cross correlation, between the reference galaxy and the neighbouring galaxies, where,

$$H(z) = \frac{I_\gamma}{N_g} \left\{ \frac{D}{(1+z)} \right\}^{(3-\gamma)} \phi(<M_o) \qquad ...(5.2)$$

in which, I_γ is a constant (=3.78 for γ= 1.77), $D = d_L/(1+z)$, d_L being the luminosity distance, and $\varphi(<M_o)$ is the total number of galaxies of different structural types per unit volume, having absolute magnitudes brighter than M_o which corresponds to the plate limit m_o for redshift z of the reference galaxy. The whole exercise reduces to the determination of $B_{gg}*$, in answer to the question: if the cluster were placed at the redshift of the galaxy of interest what degree of the clustering is required to account for the excess counts seen around it above a limiting apparent magnitude m_o.

The assumptions inherrent in this exercise are that (1) the putative cluster is indeed physically associated with the galaxy of interest, (2) the cluster galaxies are distributed spherically around it, (3) the clusters preserve their physical extent and amplitude independent of expansion of the universe. This implies the basic assumption that the clusters formed stable bound systems long before the epochs of the galaxies under consideration, and (4) there is a universal optical luminosity function of all types of galaxies and all degrees of their clustering.

5.1.2 The Optical Data

The basic source of data used here consists of the PSS blue, UK Schmidt J and ESO blue plates. Due to their location at either low galactic latitudes or near the plate edges, 6 of the giant radio galaxies were not included. For the remaining 9, it was possible to scan a field of nearly $2^{\circ} \times 2^{\circ}$ roughly centred at the parent galaxy. The scanning of the plates was done using the COSMOS measuring machine in its threshold mapping mode (McGillivray and Stobie, 1984), taking a 32μm spot and 16μm pixel size and adopting a detection threshold of 10% of the sky intensity. The automated separation of galaxies from stars was carried out using the area-magnitude plots, the basic idea being that for the same area, galaxies have fainter magnitude than stars. The technique becomes inefficient for bright stars whose light is "spread out" due to the formation of diffraction spikes and haloes. The limiting magnitudes for this effect to be significant are estimated to be -15 (PSS), -14 (ESO) and -16 (UKST) on the COSMOS magnitude scale. As described below, these values correspond to blue magnitude of 13. The classification of objects brighter than these levels was done by eye and most of them (>90%) were found to be stars. The COSMOS output were kindly made available to us by Dr. J.A. Peacock.

The plot of galaxies in each of the scanned fields often showed obvious artefacts such as circular chains of "galaxies" around the bright stars. These are caused due to the automated classification of the features such as the diffraction spikes and haloes around the bright stars. To minimise such effects we have rejected circular areas lying within 2 mm of all stars that are more than a magnitude brighter than the limiting magnitudes at which the automated star-galaxy separation is stopped, as described in the previous paragraph. In some cases (roughly one per scanned field), the areas to be blanked-out had to be slightly enlarged, in order to encompass obvious artefacts seen around the brightest stars. These modifications, meant to supplement the automated star-galaxy classification, led to the final list of galaxies detected within the fields of the 9 GRGs. The farthest 3 of them have redshifts of 0.146, 0.2055 and 0.22.

<u>The Calibration of the COSMOS Plates</u>: Since the number-magnitude counts for galaxies show considerable variation from field to field, we have chosen to calibrate the COSMOS magnitude scale by tying it to the apparent magnitudes of the

GRGs themselves. Whereas for 3C236, the value of m is known from accurate photoelectric photometry (Laing, Riley and Longair,1983), only eye estimates are availble for the remaining 8 GRGs, implying an uncomfortably large uncertainty. Hence, in these cases, we have estimated the apparent magnitudes of the parent galaxies (m_{est}) from their known redshifts using the m-z relation derived for all 37 3CR radio galaxies with $z < 0.25$, present in the sample of Laing et al. (1983). Taking the redshifts and photometrically determined values of m_B from their paper, we find the following straight-line fit which allows an uncertainty of $m = \pm 0.5$ for a given redshift:-

$$\text{Log } z = 0.1883\, m_B - 4.279 \qquad \ldots(5.3)$$

Having thus calibrated the COSMOS outputs, we estimated the limiting apparent magnitudes, i.e., the completeness limit for each field from the turnover observed in the plot of the magnitude counts. For 2 of the total 9 fields, the apparent magnitude of the parent galaxy was found to be equal to or greater than the plates' estimated completeness limit. Hence both these GRGs (0211-479 and the gaint quasar 4C 34.47) were excluded from the present study.

5.1.3. Determination of B_{gg}*

The derivation of B_{gg}^* involves computation of H(z) and A_{gg}^*. In deriving these quantities we use the same input parameters as used by PP namely; $H_o = 50$ kms^{-1}Mpc^{-1}, q_o=0.5; Schechter form for the optical luminosity function; of galaxies with the characteristic absolute magnitude M^{*} = -21.0 and the slope $\alpha = -1.25$; normalisation factor ϕ^{*} = 0.0022 Mpc^{-3} and the relative proportions of different galaxy types as 0.35 (E/SO), 0.20 (Sab), 0.20 (Sbc), 0.15 (Scd) and 0.10 (Sdm).

For deriving H(z) values, we numerically integrated the optical luminosity function (Ellis, 1982) given by (M)dM = $0.92\,\phi^{*}\ X^{(1+\alpha)}e^{-X}dM$ where $X = 10^{0.4(M^{*}-M)}$, for different redshifts, between a generous lower limit for the absolute magnitude M_{min} = -25 and an upper limit M_{max}. The value of M_{max} is different for each field. It depends on the corresponding (apparent) magnitude limit and redshift of the source under study (see Section 5.1.2). The K-corrections were adopted from King and Ellis (1985).

We checked our calculations of the optical luminosity function by computing H(z) values appropriate for the Lick survey and comparing them with the corresponding values read from Fig.1a of PP. For this we used m_{lim} = 18.6 and background surface density $N_g = 1.77.10^{-5} Sr^{-1}$ (Groth and Peebles, 1977). We find that at low redshifts (z<0.1), there is a discrepancy of a constant factor of $\sim$ 2 between our values and those of PP. Since the discrepancy is constant in this redshift range, it could arise because of a difference in the adopted value of N_g. It would not affect the results, however since we will be computing the parameter $B=B_{gg}^{*}/B_{gg}$ for each field and any redshift independent terms would cancel

(Here B_{gg} is the equivalent of $B_{gg}*$ for the general galaxy background and is computed by us in an identical manner using the published value of A_{gg}; Groth and Peebles, 1977). For redshifts z>0.1, however, the discrepancy between our H(z) values and those of PP increases for higher redshifts. We attribute this to the difference in the K-corrections used (PP used K-corrections from Ellis, 1982). The differences in the K-corrections used will be negligible at small redshifts, explaining the redshift independance of the discrepancy at low redshifts. In our sample of 7 GRGs, only one source 0114-476, has a redshift large enough (z=0.146) to be affected by the differences in the K-corrections used. We shall interpret its results appropriately (Section 5.1.4).

The other required parameter, $A_{gg}*$, is derived from the expression,

$$A_{gg*} = \frac{N_{obs} - N_{bc}}{N_g \cdot \int \theta^{-0.77} d\Omega} \qquad \ldots(5.4)$$

obtained by integrating the expression for the 2-point angular cross correlation function. Here, N_{obs} is the total number of galaxies inside the chosen area around the galaxy of interest. The angular radius of the area was taken to correspond to 1 Mpc at the redshift of the galaxy. N_{bc} is the expected number of background galaxies in the same area, the integral also being over the same area. It was calculated numerically in cases where one or more regions had to be blanked out within the area (Section 5.1.2). The radius of

1 Mpc was chosen so as to cover the boundary of any possible clustering around the GRGs. As reasoned out in PP, a radius defined in angular units would introduce redshift dependent errors.

N_{obs} was obtained by counting all the galaxies within a circle of radius 1 Mpc having magnitude above the (estimated) plate limit (Table 5.1.1). To get a reliable estimate of the background surface density, N_g, the counts must be made in regions which are far removed from the reference galaxy. Since the total plate area scanned for each GRG was only $2^o x 2^o$ in we adopted the following two procedures (see Fig.5.1): (a) all galaxies with magnitudes above the plate limit were counted outside the largest circle centred on the GRG that could be fitted within the field, and (b) the regions for making counts were chosen as circular annuli with a minimum radius of 4 Mpc for all GRGs except NGC 315 (r_{min}=1 Mpc, r_{max}=1.7 Mpc), DA 240 (r_{min} = 3 Mpc, r_{max} = 3.2 Mpc) and NGC 6251 (r_{min} = 2 Mpc, r_{max} = 2.3 Mpc). The 3 exceptions were necessiated by the limited field size available. The maximum radius in every other case was the same as in (a). The values of N_g obtained in the two ways were mostly consistent to within $\sim$30% and were, therefore averaged. In Fig.5.1a for NGC 315, it can be seen that there is a curious large-scale excess of 'galaxies' all along the western edge of the field. A check in the Zwicky catalog failed to reveal a corresponding excess. The excess could most probably be due to vignetting at the plate edge. We

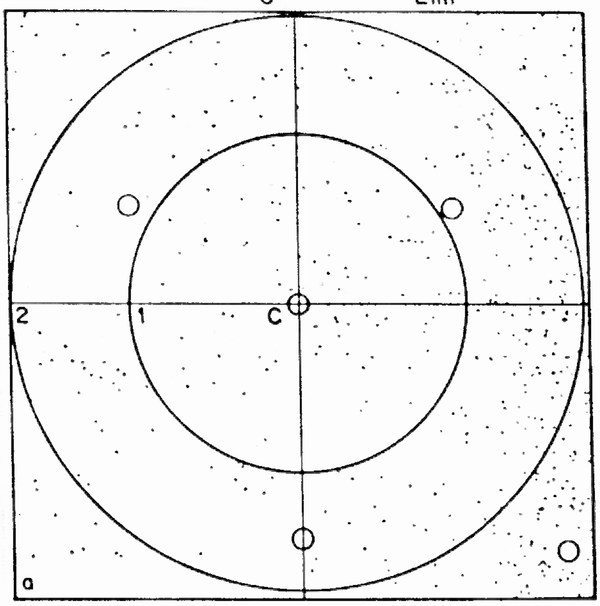

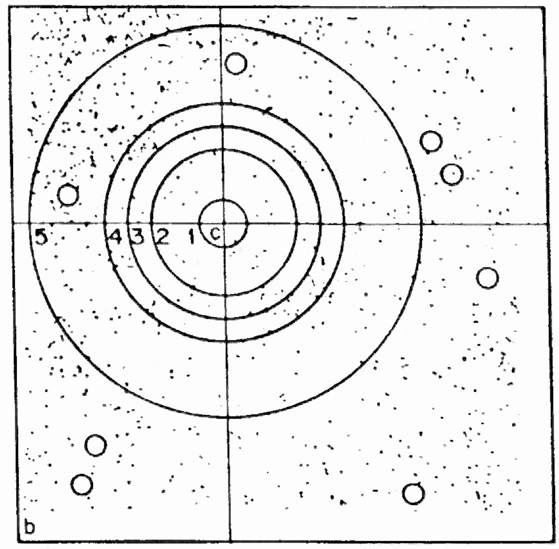

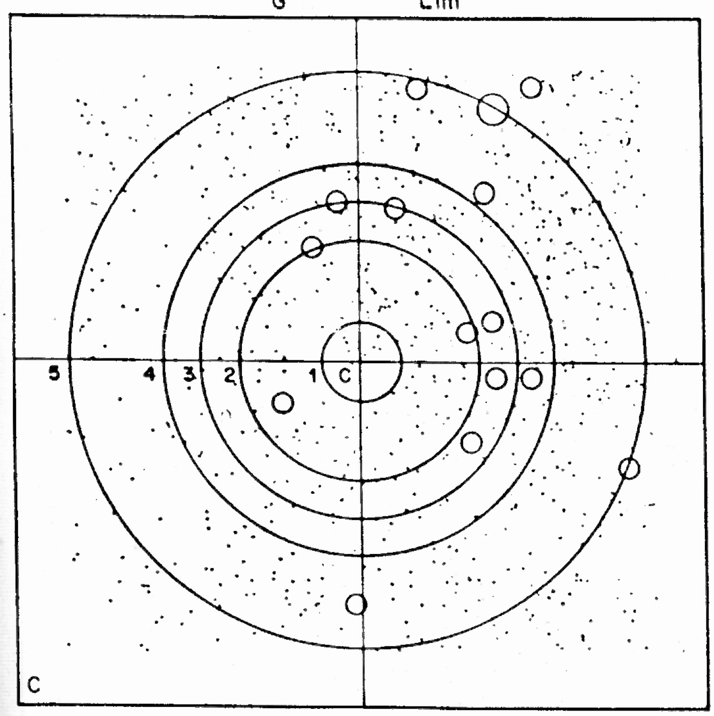

Fig.5.1.1 The optical field scanned for each GRG. The galaxies (shown as points) have magnitudes above the completeness limit (Table 5.1.1). The centre of the circles always coincide with the parent galaxy. The large circles (numbered) are shown to indicate the regions involved in the determination of N_g. N_{obs} (see Section 5.1.3). Their radii, Cn, are given at the bottom of the panels, n being the number of the circle. The small circles indicate the regions around bright stars/galaxies that were rejected (Section 5.1.2).

DA240, Z = 0·0356, $m_G^B = 15 \cdot 0$, $m_{Lim}^B = 17 \cdot 2$

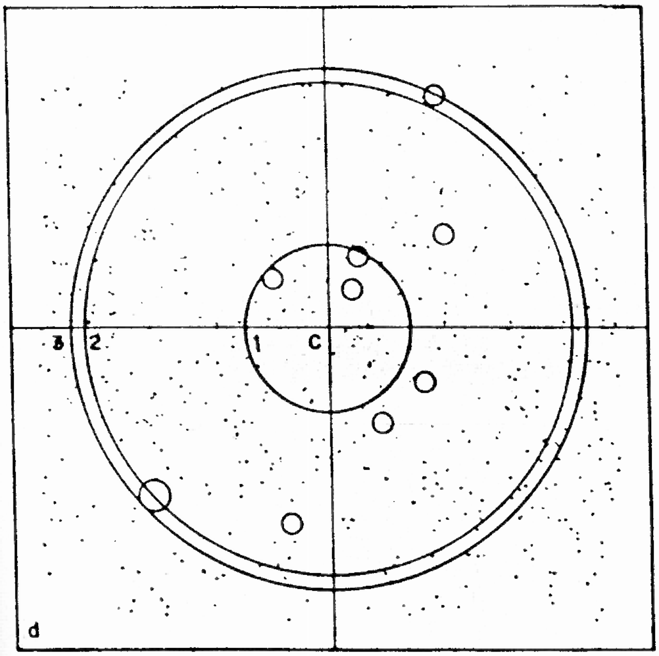

C1 = 1 Mpc C2 = 3 Mpc C3 = 3·2 Mpc

4C73·08, Z = 0·0581, $m_G^B = 16 \cdot 2$, $m_{Lim}^B = 19 \cdot 1$

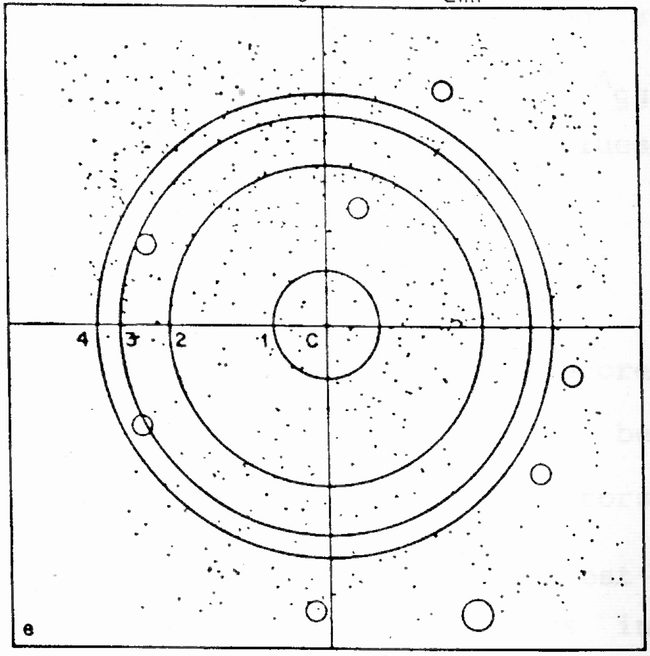

C1 = 1 Mpc C2 = 3 Mpc C3 = 4 Mpc C4 = 4·4 Mpc

3C236, Z = 0·0988, $m_G^B = 17 \cdot 2$, $m_{Lim}^B = 19 \cdot 1$

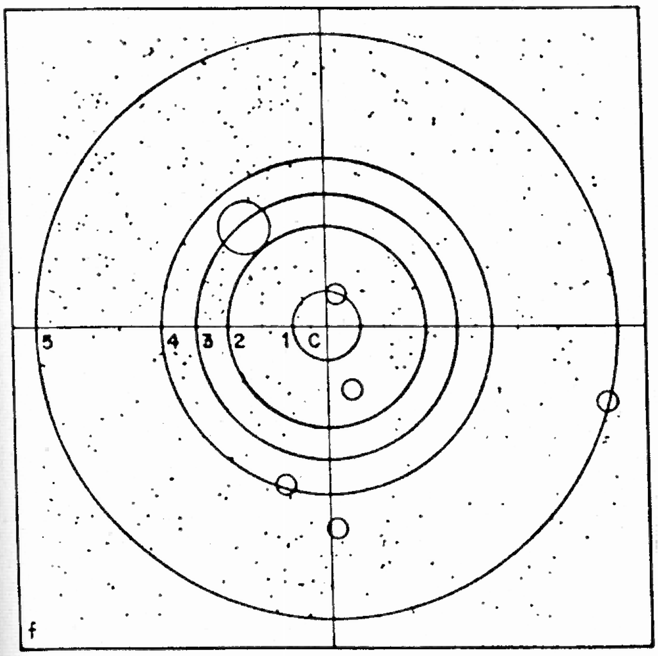

C1 = 1 Mpc C2 = 3 Mpc C3 = 4 Mpc C4 = 5 Mpc
C5 = 9 Mpc

NGC6251, Z = 0·023, $m_G^B = 14 \cdot 0$, $m_{Lim}^B = 20 \cdot 1$

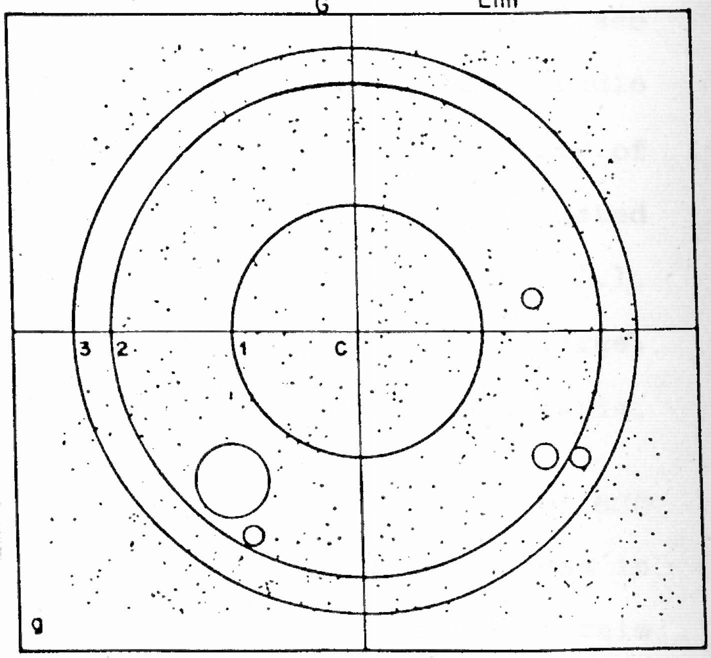

C1 = 1 Mpc C2 = 2 Mpc C3 = 2·34 Mpc

have excluded this region in all our counts. We adopted a value of 81.6 for B_{gg} (using B_{gg} = 40 obtained by PP from A_{gg} = 0.068), considering the factor of 2.04 between H(z) values derived by us and by PP for z<0.1 (see above).

5.1.4. Results and Discussion

Our results are summarized in Table 5.1.1. Before interpreting the values of B, the likely errors need to be considered. The main sources of uncertainty are : (a) errors in the estimation of N_g and (b) errors in the values of m_{est}, which would affect the plate limit estimate. The errors in these quantities get carried over to A_{gg}* and H(z) and hence in to the values of B. We estimated the error in N_g, by assuming a random distribution for the background galaxies, and by using Poisson statistics, although this is not strictly applicable since the galaxies are clustered (see PP). From our linear fit to the m_B-z plot for 3CR radio galaxies (see Section 5.1.2), we estimated an uncertainty of $\sim$0.5 mag in the magnitude estimates. The resulting estimated errors in the B values for each GRG are given in Table 5.1.1. The uncertainty in the individual B values are fairly large, as expected for the moderately deep plate material available.

As mentioned in the previous section in the case of NGC 315, we excluded the region showing the artificial excess in the galaxy counts. Such a step, however cannot totally rule out some excess contribution to the counts, although the 1 Mpc radius circle is well removed from the region of

Table 5.1.1

Source Name	NGC315	0114-476	4C40.08	DA 240	4C73.08	3C236	NGC6251
Redshift (z)	0.0167	0.146	0.078	0.0356	0.0581	0.0988	0.023
1Mpc= θ'	35.3	4.98	8.2	17.11	10.89	6.84	25.92
DMpc= $\frac{d_L}{(1+z)}$	98.96	790.43	452.99	208.06	334.11	552.2	135.66
$m^{B}_{est.}$	13.29	18.29	16.9	15.03	16.16	17.18^{+}	14.02
$m^{cosmos}_{Parent.G}$	-16.46	-14.89	-13.15	-14.16	-13.69	-13.13	-16.22
m^{cosmos}_{Lim}	-11.75	-12.25	-12.50	-12	-10.75	-11.25	-10.25
m^{B}_{Lim}	18	20.9	17.6	17.2	19.1	19.1	20.1
$N_{bg}(Sr^{-1})$	$2.04.10^{5}$	$1.38.10^{6}$	$6.31.10^{5}$	$4.64.10^{5}$	$6.21.10^{5}$	$3.56.10^{5}$	$7.9.10^{5}$
$\varphi(<M_{Lim})(Mpc^{-3})$	$1.38.10^{-2}$	$3.90.10^{-3}$	$4.65.10^{-4}$	$2.99.10^{-3}$	$5.29.10^{-3}$	$1.69.10^{-3}$	$2.34.10^{-2}$
H(z)	$1.615.10^{-3}$	$7.7.10^{-4}$	$1.06.10^{-4}$	$3.79.10^{-4}$	$8.78.10^{-4}$	$8.72.10^{-4}$	$1.07.10^{-3}$
Nobs	85	4	10	41	26	4	101
Nbc	67.44	9.12	11.34	34.5	19.6	4.23	140.1
$J/J_{original}$	2.57/2.66	0.24	0.44	1.06/1.09	0.63	0.34/035	1.73/1.82
Agg*	0.11	-0.051	0.016	0.043	0.054	-0.006	-0.094
Bgg*	68.0	-66.2	-149.0	113.5	61.5	-7.2	-87.8
B=0.0122 Bgg*	$0.83^{+0.3}_{-0.5}$	$-0.81^{+0.3}_{-0.5}$	$-1.82^{+0.4}_{-0.5}$	$1.38^{+1.2}_{-0.9}$	$0.75^{+0.8}_{-0.4}$	$-0.09^{+0.3}_{-0.1}$	$-1.07^{+0.1}_{-0.1}$

Footnotes: Row1-redshift; Row2-size conversion ratio; Row3-distance to the GRG; Row4-estimated blue apparent magnitude for the GRG parent galaxy (see section 5.1.2); Row5-GRG parent galaxy magnitude on the COSMOS magnitude scale; Row6-magnitude corresponding to the completeness limit of the plate, on COSMOS magnitude scale; Row7-blue apparent magnitude corresponding to the completeness limit of the plate; Row8-average surface density of background galaxies; Row9-optical luminosity function; Row10-computed value for H(z); Row11-number of galaxies inside the1Mpc radius circle centred on the parent galaxy; Row12-expected number of background galaxies inside a 1Mpc radius circle; Row13-value of the integralJ/J(original) - the value of J when no region is rejected inside the main area (see section 5.1.2 and 5.1.3); Row14-the angular cross correlation function; Row15-the spatial cross correlation function; Row16-Bgg*/Bgg obvious excess (see Fig.5.1.1). The value of B for NGC 315 could therefore be slightly over estimated.

In the case of 0114-476 (z=0.146), the effect of the different values of K-corrections used by us and by PP must be considered (see Section 5.1.3). It was noted above that such differences are significant only for z>0.1. For 0114-476, a difference of $\sim$11% in the estimate of B is caused due to the different K-corrections used here.

Finally, comparing the B_{gg}* values for the 4 GRGs common to our sample and the Lick sample (68 sources; Table 5 in PP) we find them to be discrepant (i.e., outside the combined error) in the cases of DA240, NGC6251 and 3C236. Similar discrepancies are seen between the Lick and Schmidt samples of PP for their 5 common sources. The discrepancy for the 3 GRGs could mostly be due to the differences in the background estimates (N_g; as was shown to be the case by PP for their 5 common sources). PP estimated the background in regions 3°-5° away from the GRG for their Lick sample. In our estimates of N_g however we were limited to regions $\sim 1^{\circ}$ from the GRG. In the case of NGC6251, the large negative value obtained by us for B_{gg}* could be due to the following reason: the GRG is known to be a member of the loose cluster (Young et al., 1979). If the background estimate is obtained near the source, its value could be higher than the value obtained around the source, if it is at the edge of the cluster. Due to the large expected errors in individual estimates of B any comparison would only be valid in a statistical sense.

Having arrived at the estimates for errors in the values of B for the 7 GRGs, we compare our results (Table 5.1.1) with the conclusions of PP based on their Table 4. The average value of B computed for all the 7 GRGs is -0.83 $\pm$0.08. From Table 4 of PP, the average B values of FRII and FRI type radio sources in their Schmidt sample of total 15 sources (which was analysed using the COSMOS machine) are 1.14$\pm$0.17 (FRII; 6 sources) and 3.05$\pm$1.10 (FRI; 9 sources), respectively.

It is thus seen that, on an average, GRGs lie in regions no denser than the environments of edge-brightened (FRII) radio galaxies. Environments as rich as those of the edge darkened (FRI) sources are clearly not indicated. Such a result was known only qualitatively so far (Waggett, 1977; Hine, 1979).

Since the large-scale gaseous environments of GRGs and normal size FRII sources appear to be similarly tenuous, the reasons, for the exceptional sizes of the GRGs could be: either they have relatively long ages, in which time (with typical intrinsic parameters) they have grown to their present sizes, or they have relatively powerful beams so that in the same time, they could grow to large sizes. Spectral index distribution studies of GRGs reveal their typical ages to be 5.10^7 yr (see Chapter II and references therein), and those of normal size sources to be a few times smaller (Alexander and Leahy, 1987). Although difference in ages could be responsible to some extent for the difference in sizes, the more likely reasons for the enormous sizes of GRGs is their higher intrinsic beam thrust (see Chapters III and VI).

5.2 ASYMMETRY STUDIES

5.2.1 Procedure

As outlined in the Introduction, we explore here the cause of the pronounced structural asymmetry frequently encountered in the case of GRGs. From the study presented here, we find that although unequal beam powers or thrusts could produce asymmetric structures, the most apparent cause seems to be an asymmetric large scale environment.

Since the median asymmetry, i.e., arm-length ratio, for FRII sources in the 3CR sample (Laing et al 1983) is 1.4 (Macklin, 1981), we label a radio galaxy as being highly asymmetric if the extent of one of the radio lobes is $\geq$40% larger than that of the other lobe. The lobe extent is defined as the separation of its outer hotspot/warmspot (or 3 σ contour) from the parent galaxy. With this criterion, 6 of the 9 GRGs for which COSMOS digitisations are available (Section 5.1), qualify as being highly asymmetric (Table 5.2.1).

To explore the possibility of differences in the external gas density on the two sides of a GRG being a cause for the asymmetry, we need a measure for the gas density at different locations around a given GRG. We adopted two quantifiers for gas density. One is, N, which is simply the count of galaxies within a standard circular area around the location of interest. The other is the count weighted by f/r, the the optical flux* of the respective galaxy divided by its distance from the location of interest. These two measures of gas density will be called 'gas density parameters' N and η, respectively.

To minimise inclusion of un-associated background or foreground galaxies we only considered galaxies lying within 2 (or, 3) magnitudes of that of the GRG (see Table 5.2.1) but excluding all those falling below the plate's completeness limit as discussed in Section 5.1. Since the radio structures several hundred kiloparsec away from the parent galaxy are more directly influenced by the local environment, rather than by the gaseous environment present in the vicinity of the parent galaxy, we adopted the following procedure: both gas density parameters were estimated for 2 circular regions of 1 Mpc radius each, centred 1 Mpc away from the GRG nucleus on opposite sides, along the radio axis of the GRG. A radius of 1 Mpc was chosen to ensure the inclusion of any associated cluster to its maximum likely bounds. Further, the selected offset of 1 Mpc from the GRG nucleus allows us to sample adequately the regions occupied by the two radio lobes#. Since both lobes of any GRG are practically at the same

* ($\log f = 3.4 - 0.4\, m_B$)

FOOTNOTE: For NGC 315 we adopted 0.5 Mpc (instead of 1 Mpc) for both the radius and the separation, in order to minimise contribution to the galaxy counts from the suspected abnormal excess counts seen near the western edge of the digitised optical field (Section 5.1).

Table 5.2.1. The asymmetry parameters for the subsample of 6 GRGs

Name	m_{lim}	m_{GRG}	$N(m_{GRG} \pm 2)$§		$\eta = \sum f/R(m_{GRG} \pm 2)$§		S_{1GHz}^{lobe} (Jy)		Relative separation of the lobe's edge from the GRG nucleus (hotspot)		(3σ contour)	
			A*	B	A	B	A	B	A	B	A	B
NGC 315	18	13.3	4	7	1.55	1.65	0.71	0.87	2.1	1.0	2	1
0114-476	20.9	18.3	1	9	1.2	3.8			1.4	1.0	1	1
4C 40.08	17.6	16.9	16	29	0.67	1.97			2.0	1.0	1.1	1
4C 73.08	19.1	16.2	15	14	1.03	1.24	1.1	2.3	1.2	1.0	1.6	1
3C 236	19.1	17.2	5	5	2.45	2.55	1.2	1.4	1.9	1.0	1.5	1
NGC 6251	20.1	14.0	5	15	3.66	9.42			1.8	1.0	2.2	1

Footnotes *A:- farther radio lobe, B:- nearer radio lobe

§For NGC 315, 0114-476 and NGC 6251, the magnitude range used in $m_{GRG} \pm 3$, otherwise N would have been too small.

distance from us, the relative optical flux densities (f) of the galaxies in the neighbourhood of the GRG are good measures of their relative optical luminosities. The latter are believed to be proportional to the visible masses of the respective galaxies (Stocke, 1979). The ratio of the optical flux of a given galaxy to its distance from a reference point (f/r), would then be a measure of its relative contribution to the gravitational potential at that point. The sum of such contributions, η , is taken to be an indicator of the gas density, at that point as discussed above. It may be noted that the galaxies contributing to the gas density parameters N and η , at the two offset locations form independent sets. This is feasible since the lobes of GRGs are so far apart.

5.2.2 Results and Discussion

The derived values of both gas density parameters, N and η , together with other relevant radio/optical parameters are given in Table 5.2.1 for each of the 6 highly asymmetric GRGs. The parameters are plotted as histograms in Fig. 5.2.1. It is seen that for 5 of the 6 highly asymmetric GRGs the asymmetry in the environment, as measured in terms of either of the two parameters, correlates with the radio structural asymmetry; the shorter lobe being on the side having an inferred denser medium. It is significant that although the parameters N and η for the remaining GRG, 3C236 do not conform to this trend, they do not exhibit the opposite trend either (Fig.5.2.1). Below, we discuss this GRG further.

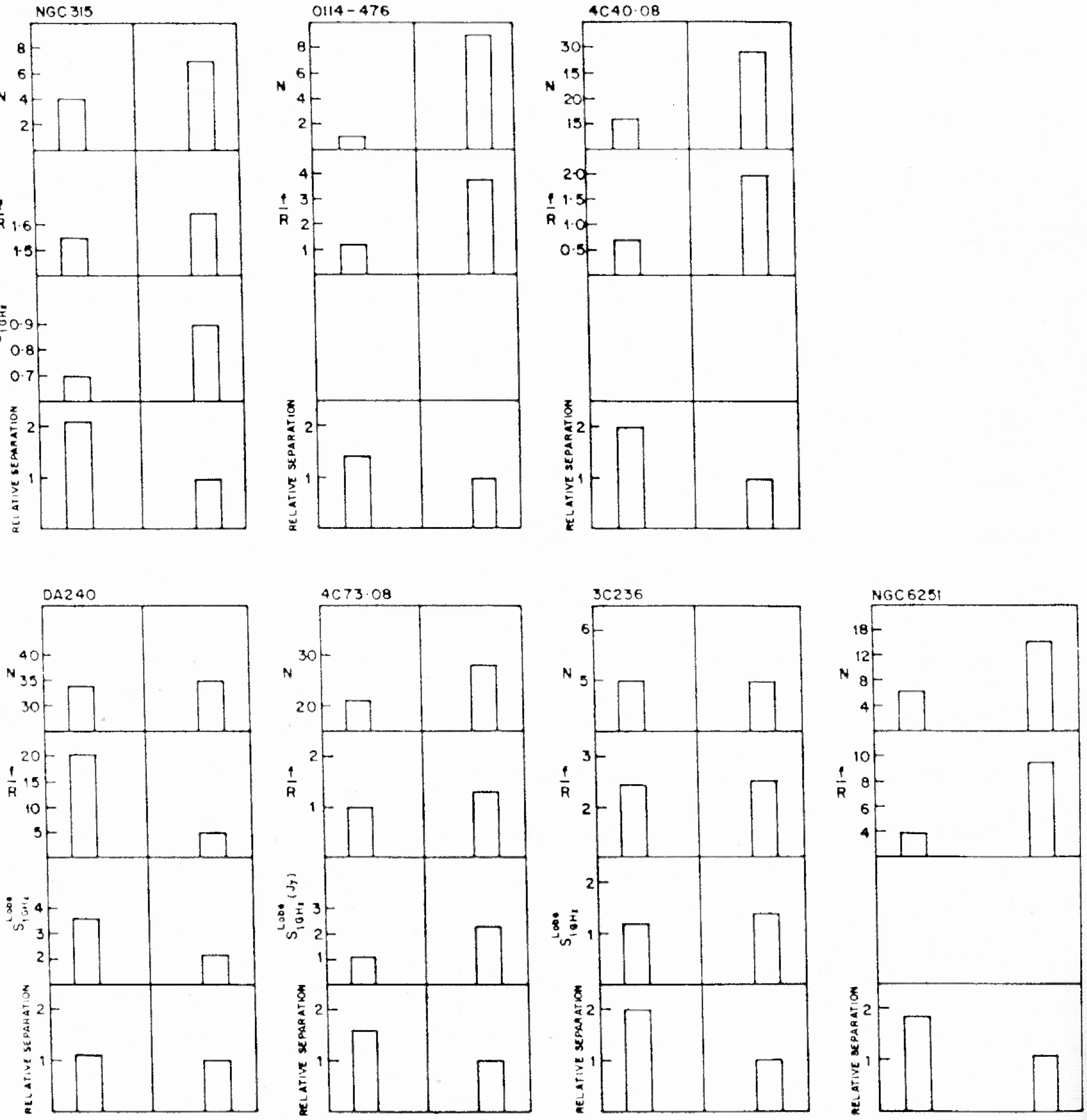

Fig.5.2.1.Comparison of parameters for the two sides in each of 7 GRGs: relative separation of the hotspots; the 1 GHz fluxes of the two lobes; the f/R values and the number of galaxies N (see Section 5.2.1).

We have also tabulated the values of total radio flux density available for the individual lobes of 3 of the GRGs (Table 5.2.1). In all these cases the higher flux density is found to be associated with the lobe with smaller length. This result is consistent with the correlation between the structural asymmetry and the asymmetry in galaxy environment, assuming that both N and η are, in fact, indicative of gas density. For instance, by combining the idea of hotspot's confinement due to the external ram pressure with the synchrotron theory, Rawlings and Saunders (1988) have argued that for a fixed beam power and liniar size, the radio luminosity of a classical double source would roughly scale as the square root of the external gas density. Thus, the effect of a couple of times denser medium on one side of the nucleus would be to increase the radio output from the lobe on that side and, at the same time, retard the growth of its linear size, by amounts adequate to explain the correlations found here.

Although the lack of COSMOS data prohibited us from including the highly asymmetric GRGs 0503-286 and 3C326 (Table 2.5;Chapter II), here too we find the same correlation between the galaxy distribution around the nucleus and the lobe asymmetry. For these cases, the galaxy distribution was evaluated by an eye examination of the PSS prints (Saripalli et al., 1986; Saripalli and Gopal Krishna, 1987).

The results presented above, lead us to suspect that the cause of the unequal extents of the GRG lobes is often related to the large scale environment of their parent galaxies, namely the asymmetric distribution of galaxies on the sides of the two radio lobes. The correlations presented above (Fig.5.2.1) could then be understood in terms of a stronger deceleration of the beam head, caused by a higher external gas density associated with the higher galaxy concentration on one side of the parent galaxy, compared to the other side. It may be noted that the asymmetry of gas density need not imply an asymmetry in the ambient pressure as well. The pressure of the media on the two sides of the parent galaxies could be well balanced and probably in an overall equilibrium with the pressure of any diffuse inter-galactic medium (IGM) filling the inter-cluster space.

Earlier, Stocke (1979) provided empirical evidence for gas to be associated with galaxy groupings. He reported correlations of radio source structure with a parameter indicative of the external gas density, derived by quantifying the distribution of the galaxies in the neighbourhood of the radio galaxy. He could account for the exceptional sizes of 4 GRGs in his sample in terms of the very low value of the gas density parameter, as compared to the value estimated for smaller radio sources in his sample. It may be noted that from X-ray observations, even some small groups of galaxies have been found to possess intergalactic gas with densities as high as $\sim 4.10^{-3} cm^{-3}$ at temperatures of $\sim 5.10^{6} K$ (Biermann et al., 1982). More recently, Burns et al., (1987) concluded that substantial amounts of gas are present in several poor groups. From the study of diffuse radio sources associated with these groups, gas densities of $\sim 2.10^{-4}.cm^{-3}$ have thus been estimated by them within such groups of galaxies.

In the literature, several mechanisms have been invoked to explain the lobe asymmetry in double radio sources. For instance, projection effects could cause a symmetric, expanding double source to appear asymmetric (Ryle and Longair, 1967; see however, Fokker,1986). Swarup and Banhatti (1981; also Ekers, 1982) suggested variations in the external medium as the likely cause for the asymmetry in the extents and fluxes of the radio lobe pair. In NGC6251, Jones (1986) even argued that the large difference between its lobe extents could be due to intrinsically different beam efficiencies in the energy transport. In the light of our result such a difference in beam efficiencies could arise due to different ambient gas densities on the two sides; the basic intrinsic parameters of the beams need not be asymmetric. However, in the case of 3C236, we do not have any evidence for asymmetry of gas density parameters, despite the observed large lobe-asymmetry (Fig.5.2.1). The reason for the asymmetry of this source is probably intrinsic. VLBI measurements by Barthel et al. (1985) clearly indicate unequal opening angles for the beams on the two sides, the better collimated beam appearing on the side of the longer radio lobe, as expected from simple beam dynamics.

5.3 CONCLUSIONS

From our study of the large optical fields around 9 GRGs, based upon COSMOS digitisations of the optical plates, we quantitatively infer that:-

(1) GRGs lie in galaxy environments similar in sparseness to those of FRII radio galaxies (statistically). They seem to avoid environments as rich as those inferred by Prestage and Peacock (1987) for FRI radio galaxies.

(2) A major cause for the frequent occurance of highly asymmetric radio structures in GRGs is the asymmetric galaxy distribution on Mpc-scale about the parent galaxy. GRGs being physically so large, neither their parent galaxies themselves, nor their envelopes are expected to create environmental asymmetry for the lobes; the cause is probably largely external. the simplest interpretation of the correlations noted in the study, would suggest that the number density of galaxies in groups of galaxies can be a useful measure of the gas density within the groups.